APPLIED PHYSICS LETTERS **100**, 142108 (2012)

Free carrier accumulation at cubic AlGaN/GaN heterojunctions

Q. Y. Wei,[1] T. Li,[1] J. Y. Huang,[1] F. A. Ponce,[1] E. Tschumak,[2] A. Zado,[2] and D. J. As[2]
[1]*Department of Physics, Arizona State University, Tempe, Arizona 85287-1504, USA*
[2]*Department of Physics, Universität Paderborn, D-33098 Paderborn, Germany*

(Received 24 February 2012; accepted 19 March 2012; published online 3 April 2012)

Cubic $Al_{0.3}Ga_{0.7}N$/GaN heterostructures were grown by plasma-assisted molecular beam epitaxy on 3C-SiC (001) substrates. A profile of the electrostatic potential across the cubic-AlGaN/GaN heterojunction was obtained using electron holography in the transmission electron microscope. The experimental potential profile indicates that the unintentionally doped layers show n-type behavior and accumulation of free electrons at the interface with a density of $5.1 \times 10^{11}/\mathrm{cm}^2$, about one order of magnitude less than in wurtzite AlGaN/GaN junctions. A combination of electron holography and cathodoluminescence measurements yields a conduction-to-valence band offset ratio of 5:1 for the cubic AlGaN/GaN interface, which also promotes the electron accumulation. Band diagram simulations show that the donor states in the AlGaN layer provide the positive charges that to a great extent balance the two-dimensional electron gas. © *2012 American Institute of Physics*. [http://dx.doi.org/10.1063/1.3700968]

GaN and its alloys are of much interest for applications in electronic and optoelectronic devices.[1] These materials typically have the wurtzite structure with space group $P6_3mc$, which exhibits large spontaneous and piezoelectric polarization fields, hence a significant quantum-confined Stark effect that limits the free-carrier recombination efficiency. On the other hand, the cubic phase of GaN with space group $F\bar{4}3m$ exhibits no spontaneous polarization and has been a subject of study for the past two decades.[2–4] Furthermore, all piezoelectric polarization components (along the growth direction and in the growth plane) should vanish for cubic films grown along a $\langle 100 \rangle$ direction,[5] which is a different case from the wurtzite GaN where the total polarization is never zero for any orientation.[6] The absence of polarization effects is one of the advantages of cubic group III nitrides over the hexagonal group III nitrides. However, there is limited experimental understanding of the electronic band structure of cubic nitride heterostructures. In particular, accumulation of carriers at the AlGaN/GaN interface has been observed but its origin is not well understood. We report here the results of a study of the electrostatic potential variation and the origin of two-dimensional electron gas (2DEG) accumulation in cubic AlGaN/GaN heterojunctions, using a combination of transmission electron microscopy, electron holography, and cathodoluminescence spectroscopy.

A cubic $Al_{0.3}Ga_{0.7}N$/GaN heterostructure was grown by plasma-assisted molecular beam epitaxy (MBE) on 3C-SiC (001) substrate,[7] with GaN and AlGaN layer thickness of 600 nm and 30 nm, respectively. The layer thickness and aluminum composition are close to the value of optimized wurtzite AlGaN/GaN heterostructures with high 2DEG density.[8] Because of the high conductivity of the 3C-SiC substrates, the doping concentration in our samples could not be obtained from Hall effect measurements. Capacitance-voltage (C-V) measurements on cubic AlGaN/GaN metal-oxide-semiconductor (MOS) structures[9,10] and on Schottky barrier devices[11–13] showed a background carrier concentration for the cubic GaN layer of about 9×10^{16}–$2 \times 10^{17}\,\mathrm{cm}^{-3}$ and for the AlGaN epilayers of about 1–$4 \times 10^{18}\,\mathrm{cm}^{-3}$, respectively. Secondary ion mass spectroscopy measurements[10] indicated that oxygen may be the reason for this background carrier concentration. In analogy to the discussion of the growth of hexagonal AlGaN with plasma-assisted MBE (Ref. 14), we suspect the nitrogen gas used in the plasma source as the source of oxygen; however the Al and Ga sources cannot be excluded.

Cathodoluminescence (CL) spectra were obtained at near liquid helium temperatures, in a scanning electron microscope operated at an electron acceleration voltage of 5 kV with a beam current of 400 pA. Cross-sectional thin samples were prepared for transmission electron microscopy (TEM) using standard mechanical wedge polishing and argon-ion milling techniques. The electron holography measurements were performed on a Philips CM200 field-emission transmission electron microscope operating at 200 keV and equipped with an electrostatic biprism. All electron holograms were recorded using a charge-coupled device camera. The electron holography measurements were performed to study the electrostatic potential profile of the cubic AlGaN/GaN heterostructure. In electron holography, the phase of the electron passing through the sample is affected by the electrostatic potential in the crystal. The phase shift in the electron beam traveling across the specimen, with respect to the electron beam in vacuum, is $\phi(x,y) = C_E V(x,y) t$, where C_E is constant for a fixed electron accelerating voltage ($C_E = 0.00728$ rad/V nm for 200 keV electrons), $V(x,y)$ is the projected electrostatic potential of the sample, and t is the sample thickness.[15] Using the holographic method, we digitally retrieve the phase shift $\phi(x,y)$ from the original hologram, acquire the distribution of the electrostatic potential $V(x,y)$, and integrate along the growth plane to obtain the one-dimensional potential profile. More details about electron holography measurements for two-dimensional electron and hole gases in group III nitride heterostructures can be found elsewhere.[16,17]

Fig. 1(a) is a cross-section TEM image of the cubic $Al_{0.3}Ga_{0.7}N$/GaN heterostructure. The crystal defects are mainly microtwins along {111} planes, which are common

 © 2012 American Institute of Physics

Downloaded 03 Apr 2012 to 131.234.170.10. Redistribution subject to AIP license or copyright; see http://apl.aip.org/about/rights_and_permissions

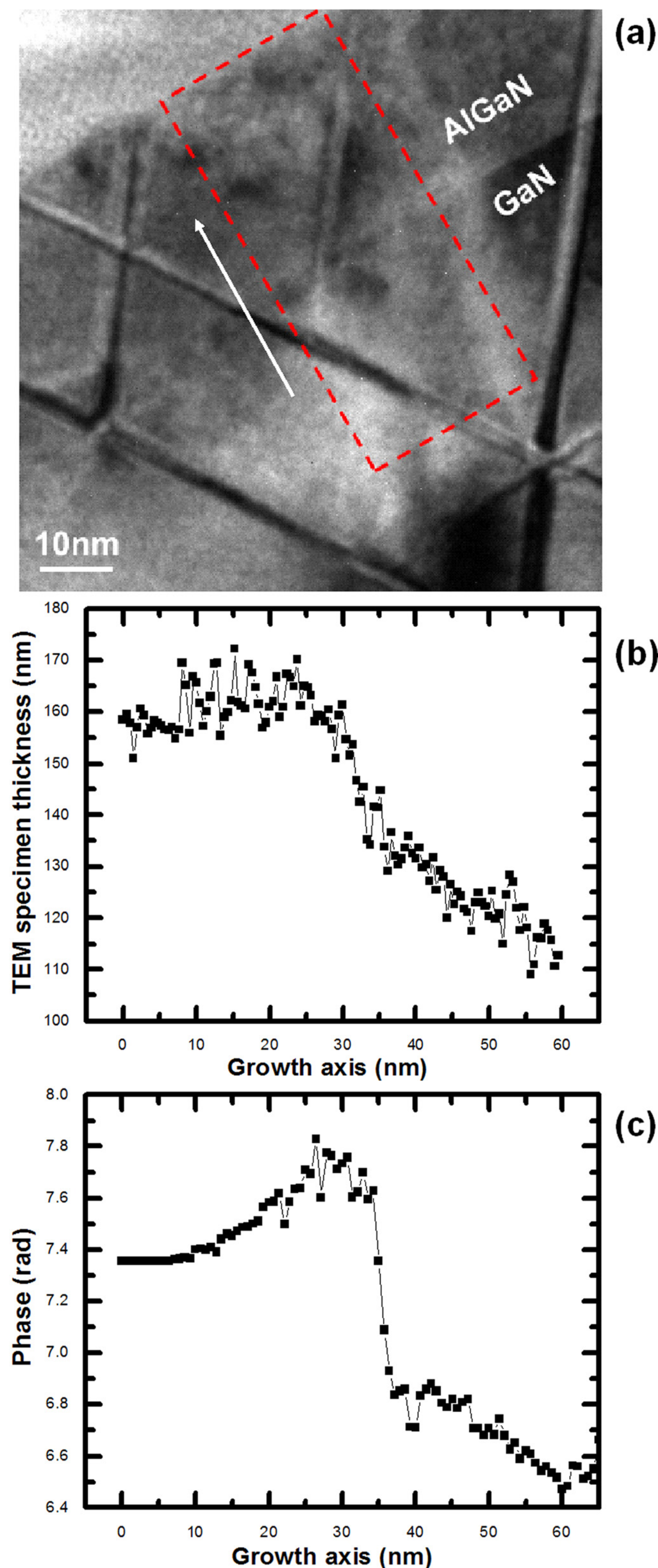

FIG. 1. The AlGaN/GaN heterostructure in cross section: (a) TEM image along a ⟨110⟩ projection showing microtwins typical in cubic GaN epitaxy; the [001] growth direction is indicated by an arrow. (b) Thickness and (c) phase profiles obtained from an electron hologram corresponding to the outlined region in (a).

in cubic thin films.[18,19] Electron holography was performed on the region marked by the rectangle, and the integrated thickness and phase profiles are shown in Figs. 1(b) and 1(c). The TEM specimen has a uniform thickness in the GaN region, but the AlGaN layer becomes thinner toward the surface. This is due to preferred oxidation and removal of the Al-containing region during ion milling. Thus, a polynomial fitting is applied to obtain the thickness profile in the AlGaN layer. The electrostatic potential profile is then obtained by dividing the phase shift by the thickness profiles; the result is shown in Fig. 2. In the GaN layer, the potential has a negative curvature, which indicates carrier depletion and free electrons accumulation at the GaN/AlGaN interface. The potential becomes flat in GaN at ~20 nm away from the interface, suggesting the free electrons are confined within that range, hence have a quasi-two-dimensional characteristic. A sheet carrier concentration $5.1 \times 10^{11}/\text{cm}^2$ is obtained from the potential curvature using Poisson's equation; this value is about one order of magnitude smaller than the density of typical wurtzite GaN 2DEG.[16] The obtained electrical data are in good agreement (within a factor of two) with conventional C-V measurements on these cubic AlGaN/GaN heterostructures and MOS structures.[9,12,13] A positive curvature of the potential energy profile in the AlGaN region is also observed, indicating an ionized donor density which is not negligible. The electron holography measurement of the potential profile has an overall error of 15% in this experiment, mainly from the estimation of thickness and from residual diffraction contrast effects.

To better understand this quasi 2DEG in cubic AlGaN/GaN, more information about the band-edge of cubic nitrides is needed. Figure 3 shows the cathodoluminescence spectrum of the sample taken at liquid helium temperature (4 K). Three separated lines at 3.29, 3.17, and 3.09 eV correspond to GaN band-edge emissions. The 3.29 eV peak is assigned to an excitonic transition in cubic GaN, while the 3.17 eV and 3.09 eV peaks are assigned to a donor-acceptor recombination and its phonon replica, in good agreement with other reports.[20–22] The AlGaN peak is at 3.95 eV with a full-width-at-half-maximum (FWHM) of 176 meV and can be fitted by three Gaussian curves. These peaks are not as well resolved

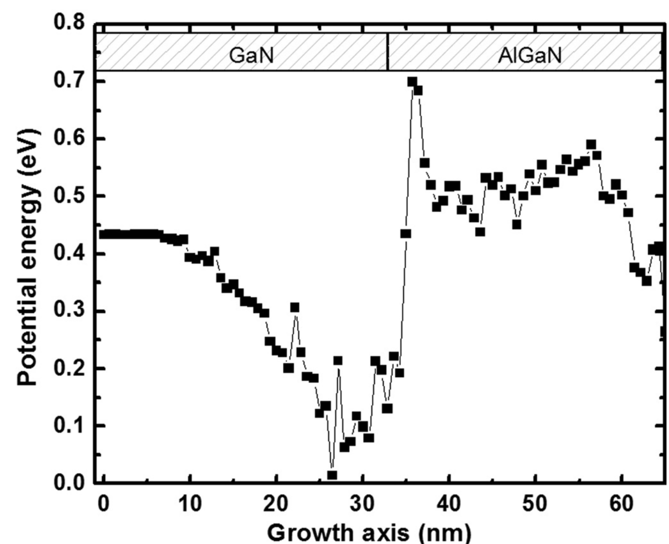

FIG. 2. Potential energy profile obtained by dividing the phase and amplitude profiles from the electron hologram. The 2DEG is characterized by a negative curvature in the potential energy profile with a density of $5.1 \times 10^{11}/\text{cm}^2$ calculated using Poisson's equation. A positive curvature in the AlGaN potential energy profile is also observed, indicating a significant ionized donor density.

Downloaded 03 Apr 2012 to 131.234.170.10. Redistribution subject to AIP license or copyright; see http://apl.aip.org/about/rights_and_permissions

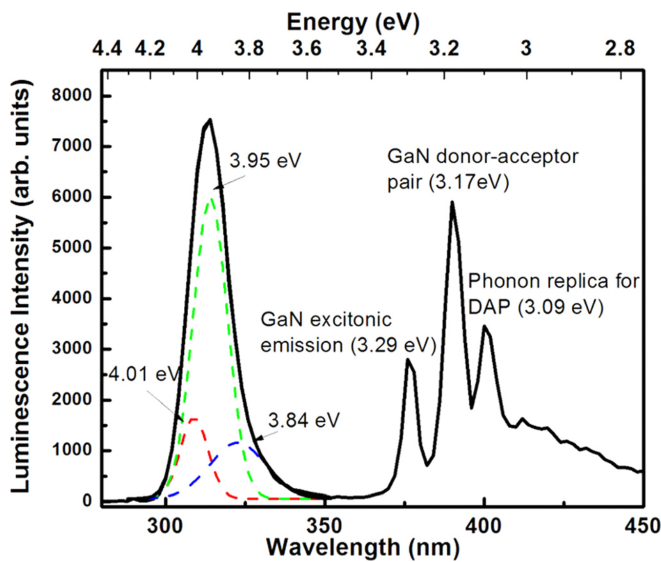

FIG. 3. Cathodoluminescence spectrum of the cubic AlGaN/GaN heterostructure at a temperature of 4 K. The spectrum shows a broad AlGaN emission at 3.95 eV with a FWHM of 176 meV and three separate GaN near-band-edge peaks.

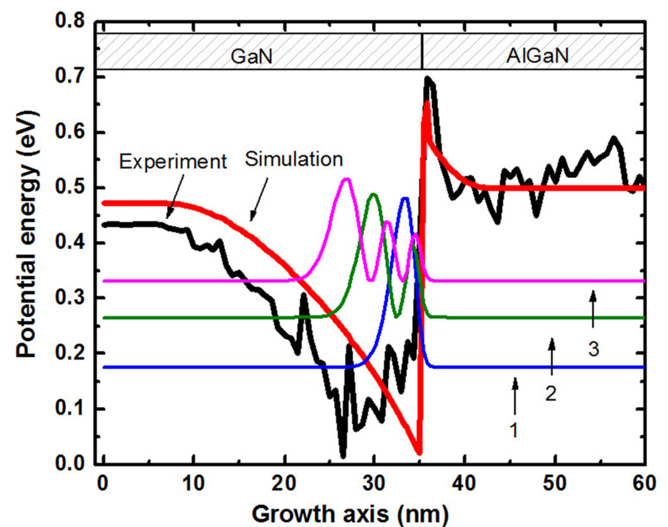

FIG. 4. Simulated conduction band profile compared with the electrostatic potential obtained by electron holography. First three electron states are also shown. The n-doping level of AlGaN is set at $2 \times 10^{18}/\text{cm}^3$.

as the GaN band-edge peaks (with ~40 meV FWHM), probably due to alloy fluctuations and residual oxygen contamination. The peak at 3.95 eV gives a band gap difference between cubic AlGaN and GaN of 0.78 eV, consistent with the nominal composition of the AlGaN film.

An interesting observation is that the difference in band gap between AlGaN and GaN is 0.78 eV in Fig. 3, while the electrostatic potential of AlGaN and GaN has an offset of ~0.65 eV in Fig. 2. The potential energy determined by electron holography can be understood as the conduction band for our case since the unintentionally doped nitride is typically n-type, and holography measurements provide a profile of the electrostatic potential experienced by the electrons in the conduction band. Hence, our experimental results suggest a conduction-to-valence band offset ratio at least as large as 5:1 for cubic AlGaN/GaN, while the first-principle calculations predict a value of 3:1 for cubic AlN/GaN.[23] With our measured energy band values, the electronic band diagram can be calculated by solving the Poisson and Schrodinger equations self-consistently, where charge neutrality from donors and free electrons are satisfied. The simulated potential energy profile compared with the experimental data is shown in Fig. 4. In the simulation, an effective n-doping level of $2 \times 10^{18}/\text{cm}^3$ in the AlGaN depletion region is used, and a zero polarization field for cubic nitride is assumed. The first three electron states are also shown in the figure, which indicates the carriers' distribution is limited in a characteristic length less than 20 nm in a quasi-2-dimensional nature. The consistency of experimental and theoretical data demonstrates that the free electron accumulation is induced by the donor states in the AlGaN layer and promoted by the large conduction band-offset of the cubic AlGaN/GaN.

We next discuss further aspects of the polarization charge effects. One important feature of the cubic nitride structure is its zero spontaneous polarization due to the higher crystal symmetry, in contrast with its piezoelectric polarization that depends on the growth orientation. For pseudomorphic heteroepitaxial growth, the biaxial strain is due to the lattice mismatch between the epilayer and substrate. For arbitrary growth facets, the strain and the piezoelectric tensors can be transformed by using a rotation matrix. The epitaxial growth is traction-free, which means the stress along the growth direction is zero. Under these conditions, the polarization field in the AlGaN/GaN heterostructures can be calculated for arbitrary crystal orientations. Figure 5 shows the calculated polarization fields for AlGaN grown on GaN as a function of polar angle, where the polar angle is defined with respect to the (001) plane. The polarization along the growth direction is maximum for a ⟨111⟩ growth direction, while the polarization component along the growth plane is maximum for a ⟨110⟩ growth direction. For a ⟨001⟩ growth direction, both perpendicular and in-plane polarization values are zero. However, if a residual

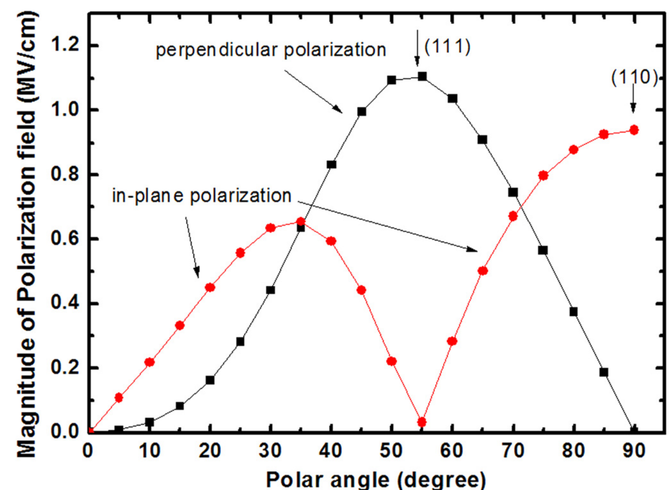

FIG. 5. Calculated polarization fields as a function of crystal orientation for a cubic $Al_{0.3}Ga_{0.7}N$/GaN heterojunction. The polar angle is defined with respect to the (001) plane. The polarization value along the growth direction is maximum for a (111) growth plane, while the polarization component on the growth plane is maximum for a (110) growth plane. For a (001) growth plane, both perpendicular and in-plane polarization are zero.

Downloaded 03 Apr 2012 to 131.234.170.10. Redistribution subject to AIP license or copyright; see http://apl.aip.org/about/rights_and_permissions

hexagonal phase exists during cubic epitaxial growth, there could be a local polarization discontinuity which introduces electric dipole moments. In TEM images as in Fig. 1(a), we observe thin hexagonal regions due to stacking faults at the boundaries of the {111} microtwins that can lead to an abrupt potential drop within a few atomic monolayers, but not to a macroscopic field. Therefore, the dipole moment due to microtwins should have a negligible effect in our case. It should be noticed that the residual hexagonal regions, in sufficient high densities, could produce polarization fields that significantly modify the band diagram.

In conclusion, the cubic $Al_{0.3}Ga_{0.7}N$/GaN heterojunction is found to have a 2DEG with a density of $5.1 \times 10^{11}/cm^2$, which originates from the donor states with density of $2 \times 10^{18}/cm^3$ in the AlGaN layer, probably due to residual oxygen contamination. A large conduction-to-valence band offset ratio of 5:1 is observed, which enhances the 2DEG accumulation. Since the polarization field is negligible in [001] cubic structures, we demonstrate that 2DEG can be achieved in the nitride semiconductors without the need of polarization effects.

D.J.A. acknowledges financial support from the "Deutsche Forschungsgemeinschaft" (Project No. As 107/4-1) and expresses gratitude to H. Nagasawa, HOYA Corporation, SiC Development Center, Japan, who supplied the 3C-SiC substrates.

[1]F. A. Ponce and D. P. Bour, Nature (London) **386**, 351 (1997).
[2]H. Okumura, S. Misawa, and S. Yoshida, Appl. Phys. Lett. **59**, 1058 (1991).
[3]S. Miyoshi, K. Onabe, N. Ohkouchi, H. Yaguchi, R. Ito, S. Fukatsu, and Y. Shiraki, J. Cryst. Growth **124**, 439 (1992).
[4]D. Schikora, M. Hankeln, D. J. As, K. Lischka, T. Litz, A. Waag, T. Buhrow, and F. Henneberger, Phys. Rev. B **54**, R8381 (1996).
[5]D. Sun and E. Towe, Jpn. J. Appl. Phys. **33**, 702 (1994).
[6]Q. Y. Wei, T. Li, Z. H. Wu, and F. A. Ponce, Phys. Status Solidi A **207**, 2226 (2010).
[7]D. J. As, S. Potthast, J. Schörmann, S. F. Li, K. Lischka, H. Nagasawa, and M. Abe, Mater. Sci. Forum **527–529**, 1489 (2006).
[8]O. Ambacher, J. Smart, J. R. Shealy, N. G. Weimann, K. Chu, M. Murphy, W. J. Schaff, and L. F. Eastman, J. Appl. Phys. **85**, 3222 (1999).
[9]A. Zado, E. Tschumak, K. Lischka, and D. J. As, Phys. Status Solidi C **7**, 52 (2010).
[10]A. Zado, J. Gerlach, and D. J. As, Semicond. Sci. Technol. **27**, 035020 (2012).
[11]D. J. As, S. Potthast, J. Fernandez, J. Schörmann, K. Lischka, H. Nagasawa, and M. Abe, Appl. Phys. Lett. **88**, 152112 (2006).
[12]D. J. As, S. Potthast, J. Fernandez, K. Lischka, H. Nagasawa, and M. Abe, Microelectron. Eng. **83**, 34 (2006).
[13]S. Potthast, J. Schörmann, J. Fernandez, D. J. As, K. Lischka, H. Nagasawa, and M. Abe, Phys. Status Solidi C **3**, 2091 (2006).
[14]C. R. Elsass, T. Mates, B. Heying, C. Poblenz, P. Fini, P. M. Petroff, S. P. DenBaars, and J. S. Speck, Appl. Phys. Lett. **77**, 3167 (2000).
[15]J. Cai and F. A. Ponce, J. Appl. Phys. **91**, 9856 (2002).
[16]Z. H. Wu, M. Stevens, F. A. Ponce, W. Lee, J. H. Ryou, D. Yoo, and R. D. Dupuis, Appl. Phys. Lett. **90**, 032101 (2007).
[17]Q. Y. Wei, Z. H. Wu, K. W. Sun, F. A. Ponce, J. Hertkorn, and F. Scholz, Appl. Phys. Express **2**, 121001 (2009).
[18]F. A. Ponce and J. Aranovich, Appl. Phys. Lett. **38**, 439 (1981).
[19]F. A. Ponce, W. Stutius, and J. G. Werthen, Thin Solid Films **104**, 133 (1983).
[20]D. J. As, F. Schmilgus, C. Wang, B. Schöttker, D. Schikora, and K. Lischka, Appl. Phys. Lett. **70**, 1311 (1997).
[21]J. Menniger, U. Jahn, O. Brandt, H. Yang, and K. Ploog, Phys. Rev. B. **53**, 1881 (1996).
[22]G. Ramirez-Flores, H. Navarro-Contreras, A. Lastras-Martinez, R. C. Powell, and J. E. Greene, Phys. Rev. B. **50**, 8433 (1994).
[23]C. Mietze, M. Landmann, E. Rauls, H. Machhadani, S. Sakr, M. Tchernycheva, F. H. Julien, W. G. Schmidt, K. Lischka, and D. J. As, Phys. Rev. B. **83**, 195301 (2011).

Downloaded 03 Apr 2012 to 131.234.170.10. Redistribution subject to AIP license or copyright; see http://apl.aip.org/about/rights_and_permissions